LONG-PERIOD GEOMAGNETIC PULSATIONS AS AN ELEMENT OF THE SPACE WEATHER INFLUENCE ON TECHNOLOGICAL SYSTEMS

N.V. Yagova (ID)
Schmidt Institute of Physics of the Earth RAS,
Moscow, Russia, nyagova@ifz.ru
Geophysical Center RAS,
Moscow, Russia

Ya.A. Sakharov
Geophysical Center RAS,
Moscow, Russia, sakharov@pgia.ru
Polar Geophysical Institute,
Apatity, Russia

V.A. Pilipenko (ID)
Schmidt Institute of Physics of the Earth RAS,
Moscow, Russia, pilipenko_va@mail.ru
Geophysical Center RAS,
Moscow, Russia

V.N. Selivanov
Northern Energetics Research Center,
Apatity, Russia, v.selivanov@ksc.ru

Abstract. We analyze variations in geomagnetically induced currents (GIC) and pulsations of the geomagnetic field latitudinal B_y component in the frequency range 1–20 mHz. The analysis is based on the data from GIC registration at the Kola Peninsula and magnetic data from IMAGE network stations, obtained with 10 s sampling in 2017. This allows us to include pulsations of both Pc5/Pi3 and Pc4/Pi2 frequency range in the analysis and examine polyharmonic pulsations with spectral maxima in both ranges. It is shown that GICs are effectively generated at frequencies above 5 mHz. Polyharmonic pulsations are potentially more dangerous than monoharmonic ones because the ratio of GIC to magnetic field pulsations' amplitude is higher and the lifetime of unipolar GIC is longer.

Keywords: space weather, geomagnetic pulsations, geomagnetically induced currents.

INTRODUCTION

Induction of geomagnetically induced currents (GICs) in long conductors is the most dangerous and basically irreversible terrestrial effect of space weather disturbances. Among GIC effects, the most widespread are cascade shutdowns of electrical equipment. Their economic and humanitarian after-effects can be compared with the most destructive natural catastrophes [Pulkkinen et al., 2008; Love et al., 2022].

Both during magnetic storms and during magnetically quiet periods, geomagnetic pulsations are an effective source of GICs. The highest GIC amplitudes are associated with long-period Pc5/Pi3 pulsations [Apatenkov et al., 2004; Wik et al., 2008; Heyns et al., 2021]. In [Yagova et al., 2021; Sakharov et al., 2022], the ratio R_{IB} of the amplitude of GIC variations to the amplitude of geomagnetic pulsations is used to evaluate the efficiency of GIC excitation by pulsations (hereinafter referred to as GIC efficiency). The value of R_{IB} even at one point significantly depends on the spectral content of the pulsations: the GIC efficiency turns out to be higher for pulsations with several spectral maxima [Sakharov et al., 2022].

Yagova et al. [2021], by analyzing measurements of GIC pulsations and geomagnetic pulsations in the 1–5 mHz range, have found that higher values of R_{IB} are observed for pulsations in which the wave field varies slightly on spatial scales of the order of the conductor length (hereinafter referred to as large-scale pulsations). For GIC-related applications, the spatial distribution of the geomagnetic pulsation field in directions parallel and normal to the ground conductor differs in the influence and in the parameters to be taken into account. The spatial scale effect in the direction normal to the conductor is "technical" in nature and is associated with the finite distance between the magnetometer and the GIC measurement point. For pulsations with high spectral coherence and an amplitude ratio close to 1 along this direction, the data interpolation or extrapolation error will be small. Otherwise, there may occur both "false alarm" (type I error) if the pulsation amplitude near the conductor is lower than at the measurement point and "false negative" (type II error) if the amplitude of pulsations near the conductor is higher than the amplitude at the measurement point. For the direction along the conductor, the phase distribution of geomagnetic pulsations also becomes significant since in the case of a small phase difference the electromotive force is summed throughout the length of the conductor.

To quantify GICs, we have to take into account time and space characteristics of a geomagnetic disturbance [Pulkkinen et al., 2006], the distribution of ground conductivity, and parameters of electrical networks [Boteler, Pirjola, 2017]; hence the need for a ground conductivity model based on measurements of geomagnetic and electrotelluric fields with high spatial resolution [Cherevatova et al., 2015; Hartinger et al., 2020]. In realistic conductivity models, numerical simulation is used to calculate the electrotelluric field and GICs [Bedrosian, Love, 2015; Juusola et al., 2020]. Nonetheless, even for the regions where the conductivity distribution is known

with high spatial resolution there are significant differences between measured and calculated GICs [Nakamura et al., 2018]. For some regions and frequency ranges, simplified environmental models provide approximate estimates that differ little from the results of calculations in the models with quasi-real conductivity distribution [Gannon et al., 2017].

In the problem about the effect of polarization of pulsations on GIC excitation, two limiting cases can be distinguished. For the horizontally homogeneous ground conductivity, the contribution of the magnetic field component perpendicular to the power transmission line predominates, and in the opposite limiting case when the scale of the horizontal irregularity is of the order or smaller than the length of the power line, both components give a contribution of the same order. Analysis of simultaneously measured variations in GICs and geomagnetic pulsations in the auroral zone, carried out in [Sakharov et al., 2021], has shown that for a quasi-meridional power line both components contribute to the excitation of GICs, but the correlation between geomagnetic pulsations and GIC variations is higher for the latitudinal B_y component.

GIC-related electric power system disruptions occurred not only at auroral latitudes, where Pc5/Pi3 pulsations predominate, but also at subauroral and even middle latitudes [Marshall et al., 2012; Lotz, Danskin, 2017; Zhang, Ebihara, 2022]. This raises the question about GICs excited by Pc3-4 pulsations typical of these regions. In addition, irregular Pi2 pulsations and higher harmonics of lower frequency pulsations fall into the Pc4 range [Fukunishi, Lanzerotti, 1974]. In this case, disturbances with frequencies higher than the Nyquist frequency can distort the results of the analysis of the relationship between GICs and pulsations with a 60 s sampling rate [Trichtchenko, 2021; Hartinger et al., 2023].

Efficiency of GIC excitation by pulsations significantly depends on the spatial distribution of the wave field, which differs for different types of pulsations. The spatial structure of Pi2 pulsations has been studied from auroral to low latitudes [Yumoto et al., 1994; Nosé et al., 2006; Wang et al., 2017]. According to the spatial amplitude and phase distributions, several classes of Pc4 pulsations can be identified. For resonant pulsations, the spatial scale along the meridian is determined by the Q-factor of the magnetospheric-ionospheric Alfvén resonator [Baransky et al., 1995]. In this case, the main power on Earth is concentrated in the magnetic field meridional component B_x, whereas in the latitudinal component B_y the feature near the resonant shell is less pronounced [Lifshits, Fedorov, 1986]. A separate class includes high-latitude Pg pulsations, manifested mainly in the latitudinal magnetic field component and localized in a narrow latitudinal zone [Motoba et al., 2015]. Spatial distribution of the amplitude and phase of the daytime Pc3-4 pulsations, coherent at several IMAGE network stations, has been examined by Howard and Menk [2005]. The authors have identified amplitude and phase variations of several types, both corresponding to and differing from the Alfvén resonance structure. At the same time, parameters of the spatial distribution of Pc4/Pi2 pulsations, including irregular "noise" and

higher harmonics of Pc5 dominating at auroral latitudes, have not been studied with sufficient accuracy for GIC-related problems.

Danger of GICs to electrical equipment is attributed not only to extreme GICs of hundreds of amperes, which can cause direct damage [Pulkkinen et al., 2005; Boteler, 2019], but also to harmonic distortion of the industrial frequency current, which lead to incorrect operation of power system protections [Gusev et al., 2020a, b]. Calculation of the quasi-static current effect on a transformer in view of partial magnetization curves has shown that the most dangerous is the range of GIC amplitudes when the magnetization dependence on the current is already nonlinear, but saturation has not yet been achieved. Since power system protections are set for the amplitude ratio between industrial current harmonics, the probability of incorrect operation is higher for the direct current (DC) level, at which this ratio is maximum. For the power transformer model on a 500 kV line considered in [Gusev et al., 2020b], the region of the most hazardous GICs is 4–10 A. This level of GICs is typical for the Pc5/Pi3 pulsations occurring at auroral latitudes during moderate geomagnetic activity. Since the condition for incorrect operation of power system protection is the time coincidence of the transient process (both during normal operation and after a short circuit) with a sufficient level of core magnetization by DC, then, in addition to the GIC amplitude, the lifetime of unipolar current I_{asym} becomes important. To each averaging time T_1 corresponds a certain level of I_{asym} For quasi-monochromatic pulsation, the values of I_{asym} of the order of GIC variation amplitude are observed at $T_1 < T/2$, where T is the pulsation period. For GICs produced by geomagnetic pulsations with several maxima in the spectrum, T_1 may be much higher, but this parameter has not yet been studied experimentally.

In this paper, we deal with the GICs driven by geomagnetic pulsations in the frequency band from 1.5 to 20 mHz, including Pc5/Pi3 and Pc4/Pi2 ranges. For Pc4/Pi2 pulsations, we examine the relationship between the ratio R_{IB}^2 and the parameters of the field spatial distribution of pulsations whose influence has been previously confirmed for Pc5/Pi3. In addition, we analyze the effect of the spectral content of pulsations on R_{IB}^2 and the lifetime of the unipolar current for the entire range under study.

1. DATA AND PROCESSING

The analysis is based on data for 2017 since there are GIC measurements made at the station Vykhodnoj (VKH) with a time resolution of 10 s for this period. The station is included into the GIC measurement system of the quasi-meridional power line "Northern Transit", located in the north-west of the Russian Federation [Barannik et al., 2012]. We have analyzed geomagnetic pulsations, using data from three IMAGE stations [Tanskanen, 2009]. The relative position of the power line, the GIC measuring station, and magnetometers is schematized in Figure 1. Coordinates of the stations and the time of the local magnetic midnight are listed in
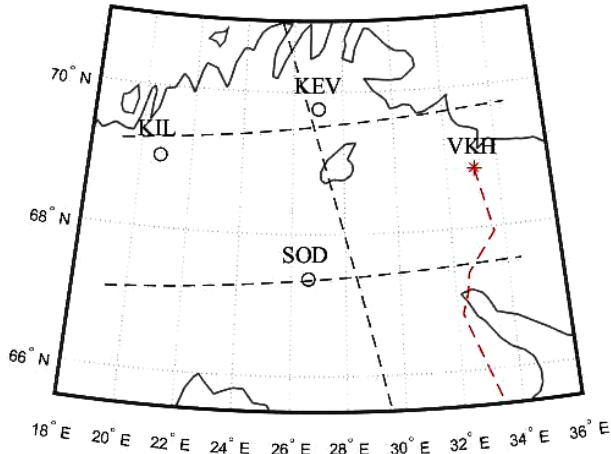
Figure 1. Layout of the power line (red dashed curve), GIC measurement station (VKH), and three stations of the IMAGE network; black dashed lines indicate geomagnetic coordinates (the Figure was taken from [Yagova et al., 2021])

Table 1. As in [Yagova et al., 2021], the wave field spatial distribution is analyzed for pairs of KEV-KIL and KEV-SOD stations, located along the magnetic parallel and meridian respectively. We examine the geomagnetic pulsations and their related GIC variations with a peak-to-peak amplitude higher than 10 A. To estimate the Power Spectral Density (PSD), spectral coherence γ^2, and phase difference $\Delta\phi$, we employ the Blackman—Tukey method [Jenkins, Watts, 1972] for an interval of 512 points (~85 min) with 10 min sampling. The method and parameters were chosen so that to ensure the generality of the method and the possibility of comparing the results with the results of previous works. As in

[Yagova et al., 2021; Sakharov et al., 2022; Sakharov et al., 2024], we delve into the relationship between GIC pulsations and the magnetic field B_y component. We have selected intervals such that the coherence between GIC and B_y variations at the frequency of the principal spectral maximum $R_{IB}^2(f_1)$ exceeds 0.5. The pulsations were considered polyharmonic if at least one spectral maximum met the condition $R_N > R_b$. Here, $R_N = P_{WN}/P_{W1}$, where 1 and N refer to the principal and any of the other spectral maxima respectively, and the function $P_W(f)$ is the spectrum that is obtained from PSD by excluding the linear trend from the log(PSD) dependence on the logarithm of frequency. The threshold value $R_b = 0.22$, which provides close numbers of intervals for pulsations with one and several harmonics and maximum contrast in relation to R_{IB} between these pulsation groups.

Inclusion of Pc4/Pi2 pulsations in the analysis raises the question about their GIC efficiency. On the one hand, if the spatial scale of the geomagnetic disturbance is large compared to the length of the conductor, R_{IB} increases with frequency f as $f^{1/2}$ for a uniformly conducting ground or even as f in a thin conducting layer model, which often turns out to be sufficient to estimate GICs on regional scales [Love et al., 2016]. On the other hand, the spatial scale of pulsations is higher for low-frequency pulsations; and when including higher-frequency pulsations in the analysis, it is necessary to estimate the pulsation field spatial distribution parameters that affect their GIC efficiency.

Table 1

Coordinates and local magnetic time of observation stations

Station code	Geographic		Geomagnetic		Universal time of the local magnetic midnight
	Latitude	Longitude	Latitude, Φ	Longitude, Λ	
VKH	68.83	33.08	65.53	112.73	20:49
KEV	69.76	27.01	66.65	108.35	21:06
KIL	69.02	20.79	66.13	102.80	21:28
SOD	67.37	26.63	64.22	106.52	21:13

To describe the wave field spatial distribution, we have used, as in [Yagova et al., 2021], five cross-spectral parameters of geomagnetic pulsations, determined from pairs of stations along the parallel (EW) and meridian (NS). For EW, we calculate the spectral coherence γ_{EW}^2 and the PSD ratio R_{EW}^2; for NS, γ_{NS}^2, R_{NS}^2, and the phase difference $\Delta\phi_{NS}$. These parameters are determined in the vicinity of spectral maxima for the intervals with over-threshold coherence γ_{IB}^2.

2. RESULTS

2.1. An example of GIC excitation by pulsations

On November 21, 2017 (day 325), a weak magnetic storm occurred with a minimum *Dst*=–42 nT at ~8 UT. The conditions before the shock wave were character-

ized by an increase in the solar wind (SW) velocity from 350 to 600 km/s, a southward rotation of the interplanetary magnetic field (IMF) (minimum B_z=–10 nT), and an increase in the SW dynamic pressure P_{SW} to almost 10 nPa. A burst in auroral activity with maximum *AE* of ~1000 nT occurred during the main phase simultaneously with minimum *Dst*. The second burst of auroral activity with *AE*=500–700 nT began around 14 UT, when the KEV and VKH stations were in the dusk sector. The GIC and geomagnetic field pulsations (B_y) and their spectra are illustrated in Figure 2 for the interval 14:20–15:40 UT. To eliminate the trend, high-pass filtration was carried out with a cutoff frequency of 0.9 mHz. Pulsations of B_y had an average peak-to-peak amplitude 20–30 nT and a maximum one to 50 nT and caused GIC pulsations with a peak-to-peak amplitude 10–15 A (see Figure 2, *a*). For polyharmonic pulsations, I_{asym} can exist for several visible pulsation periods. To illustrate this
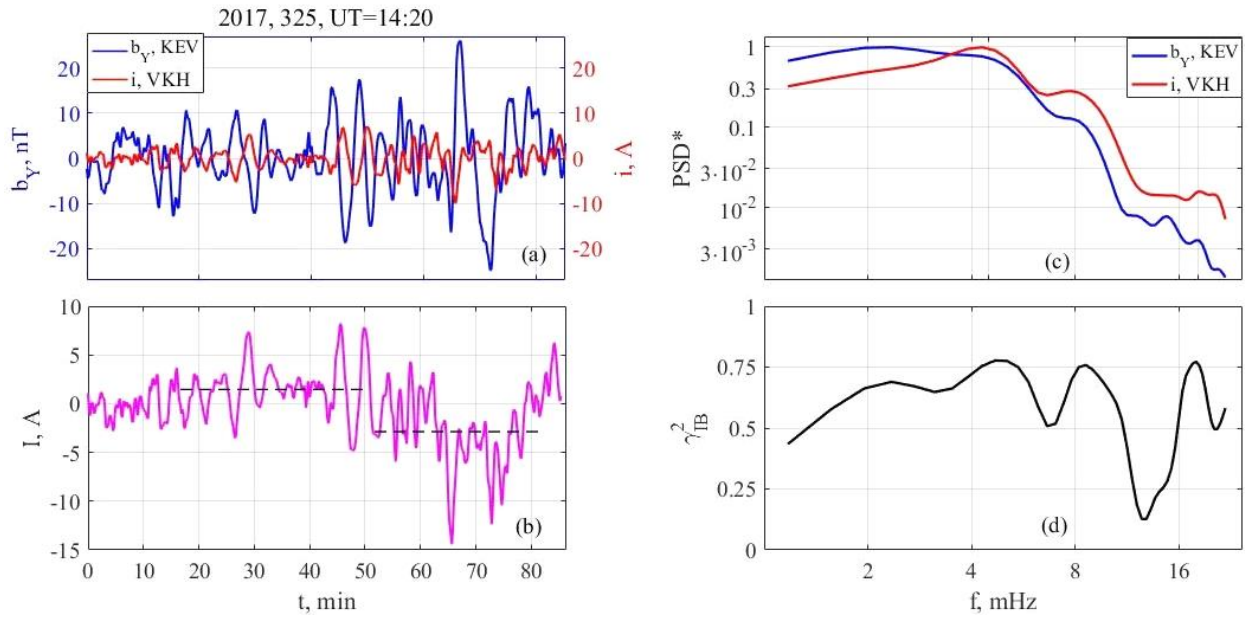
Figure 2. GIC excitation by geomagnetic pulsations on November 21, 2017: *a* — GIC pulsations (red curve) and geomagnetic field component B_y(blue curve); *b* — unfiltered GIC; black dashed lines mark the average unipolar current I_{asym}; *c* — normalized PSD; *d* — spectral coherence

effect, Figure 2, *b* exhibits original (unfiltered) GIC and average I_{asym} for two 35–40 min intervals. The I_{asym} values for these intervals are +2 A and –3 A. In the pulsation spectra of B_y and GIC, the maxima occur at 4.5 and 8 mHz, and there is also a weak maximum at 18 mHz (see Figure 2, *c*). The ratio between the amplitudes of current pulsations and geomagnetic pulsations, determined from waveforms, is 0.25–0.4 A/nT, and the PSD ratio is 2.5 times higher at the frequency of the second maximum than that at the frequency of the first (principal) maximum.

The spectral coherence $\gamma_{IB}^2 > 0.5$ for $1.5 < f < 11$ mHz and near 18 mHz. There are coherence maxima with $\gamma_{IB}^2 \geq 0.75$ in the vicinity of PSD maxima (see Figure 2, *d*).

The example considered shows that GICs are generated by polyharmonic geomagnetic pulsations such that the principal maximum frequency falls into the Pc5 range; and the harmonic frequencies, into the Pc4 range. The pulsations occur in the dusk sector during a weak magnetic storm (6–8 hrs after minimum *Dst*). An important feature of these pulsations is the existence of an unbalanced GIC up to 3 A (20 % of the GIC peak-to-peak amplitude) with approximately 10 apparent pulsation periods.

2.2. Spatial distributions of pulsations of two subbands

Let us examine statistical regularities for the GICs associated with geomagnetic pulsations in the 1–20 mHz frequency range. In [Yagova et al., 2021], the upper limit of the range in question was 5 mHz, which is somewhat lower than the limit of the nominal Pc5 range. In this study, we compare the ratio R_{IB}^2 and spatial distribution parameters for pulsations with one and several maxima in the spectrum for the 1–5.5 and 5.5–20 mHz ranges, which ensures comparable sample sizes and consistency with our previous studies. Monoharmonic pulsations (group 1) are divided into low- and high-frequency (*L* and *H*), whereas for polyharmonic pulsations (group *N*) spectral parameters are determined separately for each of the two principal maxima. As a result, we can identify mismatched intervals for groups L_1 and H_1 and partially coincident intervals for groups L_N and H_N. The number of the intervals under study and their total durations are presented in Table 2. Data on the total duration of polyharmonic pulsations depending on frequencies of spectral maxima indicates that most of the polyharmonic pulsations cover both frequency subbands so that the low-frequency maximum is in the Pc5/Pi3 range; and the high-frequency ones, in Pc4/Pi2, as in the case illustrated in Figure 2.

As follows from Figure 3, the average values of R_{IB}^2 are higher for polyharmonic pulsations, and for higher-frequency pulsations the average value of R_{IB}^2 is about twice as high as for low-frequency ones (the only noticeable deviation is observed at 9.2 mHz, where pulsations with one principal maximum exhibit $R_{IB}^2 > 0.1$ A^2/nT^2). Thus, pulsations with a high-frequency principal maximum and polyharmonic pulsations statistically demonstrate high GIC efficiency. This suggests that the percentage of large-scale pulsations for the Pc4/Pi2 range is comparable to that for the Pc5/Pi3 range.

Let us look into the distributions of the main parameters characterizing the spatial field of pulsations (Figure 4). The range-average spectral coherence $\gamma^2 > 0.5$ for both latitudinal (Figure 4, *a*) and meridional (Figure 4, *c*) directions, whereas for higher harmonics of polyharmonic pulsations for individual frequencies, the coherence

The number of events and lengths of intervals

Number of spectral maxima N_{max}	Frequency of spectral maximum (mHz)	Designation	Number of intervals	Total duration (hours)
1	≤5.5	L_1	104	51.5
1	>5.5	H_1	199	114
1	all	1	303	153
>1	$f_1<5.5$	L_N	260	128
>1	$f_2>5.5$	H_N	327	172
>1	all	N	340	172
all			643	260
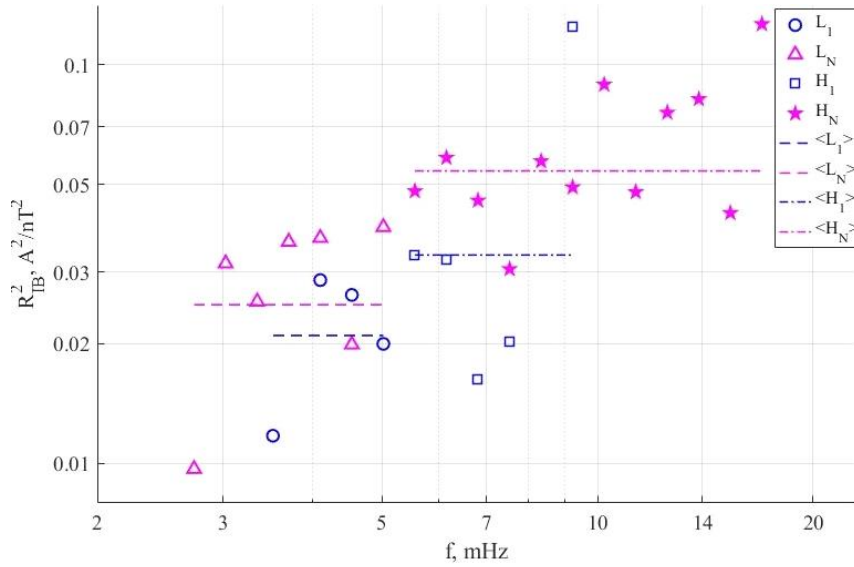
Figure 3. Annual average PSD ratio R_{IB}^2 as function of the spectral maximum frequency for mono and polyharmonic pulsations. Averages for the pulsation groups are indicated by dashed and dash-dot lines
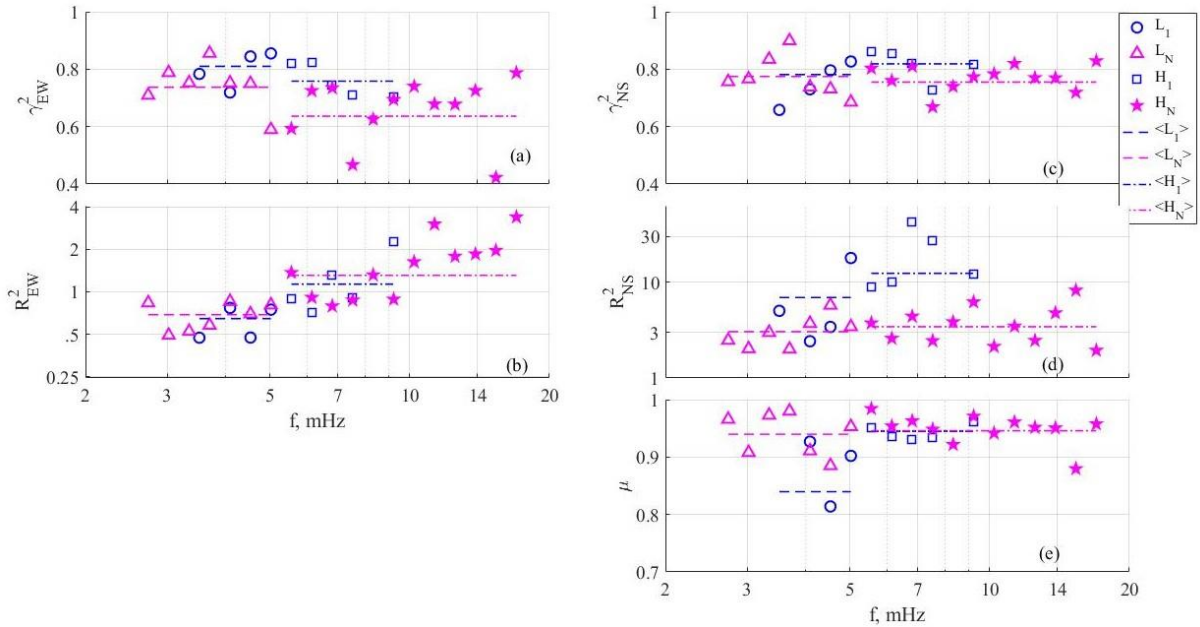
Figure 4. Annual average parameters of the pulsation field spatial distribution as function of the spectral maximum frequency and group averages: *a* — spectral coherence for the EW direction; *b* — PSD ratio in the EW direction; *c* — spectral coherence for the NS direction; *d* — PSD ratio in the NS direction; *e* — μ=cos(Δϕ) in the NS direction

is lower than 0.5. The ratio R^2_{EW} in the latitudinal direction differs from 1 no more than three times for all frequencies (Figure 4, *b*); and the range-average value, no more than 1.5 times.

The spatial distribution of the pulsation field along the power line, i.e. in the meridional (NS) direction, has the greatest impact on the efficiency of GIC excitation. The coherence values $R^2_{NS} > 0.6$ for all frequencies and the range-average values exceed 0.7 (Figure 4, *c*). The average PSD decreases from high to low latitudes, which is expressed in $R^2_{NS} > 1$ (Figure 4, *d*). Values of R^2_{NS} are higher for pulsations with a single spectral maximum than for polyharmonic ones. To account for the effect of the phase difference $\Delta\phi$ on GIC, the most informative parameter is $\mu=\cos(\Delta\phi)$ (Figure 4, *e*). The average values of $\mu>0.8$ for all frequencies, and the range-average values exceed 0.9 for all polyharmonic pulsations and H_1 pulsations. Thus, the combination of a more uniform PSD distribution along the meridian and a higher μ value makes the generation of GIC at the frequency of high-frequency maximum of polyharmonic pulsations (H_N) most effective. The GIC measurement station Vykhodnoi (VKH) lies to the east of the KEV magnetometric station; therefore, the effect of higher R^2_{IB} for H_N pulsations can be enhanced by a higher average ratio R^2_{EW} than other pulsation groups.

2.3. Lifetime of the unipolar current

To explore the dependence of average unipolar GIC I_{asym} on the averaging time T_1, we have used the original unfiltered signal and have examined T_1 from 10 min to 3 hrs. The parameters of I_{asym} are shown in Figure 5 for mono and polyharmonic pulsations. Figure 5, *a* illustrates the averaging time dependence of the I_{asym} modulus. For all values of T_1, large unipolar current values

are observed for polyharmonic pulsations. For both pulsation groups, I_{asym} varies slightly when $T_1<45$ min, and for long times it decreases according to the power law. As a result, near this boundary at $I_{asym}\approx5$–6 A for polyharmonic pulsations T_1 is about twice as high as for pulsations with one spectral maximum. For the problem of GIC effect on electrical equipment, not only the average value of unbalanced GIC is important, but also the occurrence probability of current with an amplitude higher than a given one. The dependence of the occurrence probability of $I_{asym}>3$ A on T_1 is illustrated in Figure 5, *b*. For this parameter, the difference between mono and polyharmonic pulsations is ~20 % for $T_1<40$ min. With further increasing T_1, the difference between occurrence rates of over-threshold I_{asym} increases and reaches 50 % at $T_1=80$ min.

The result presented in Figure 5, *a, b* depends both on the waveforms of current variations and on their amplitude. To exclude the amplitude effect, we took the parameter R_{asym}, defined as the ratio of I_{asym} to the 1–20 mHz GIC variation amplitude calculated from variance, as a measure of the relative magnitude of the unipolar current (Figure 5, *c, d*). The R_{asym} values are higher for polyharmonic pulsations throughout the range of averaging times. For $T_1<80$ min, R_{asym} for polyharmonic pulsations is about one and a half times greater than for pulsations with one maximum, and for long averaging times the difference decreases to 20 % (Figure 5, *c*). At the same time, the averaging time dependence of the part of the intervals with $R_{asym}>0.1$ (Figure 5, *d*) qualitatively repeats the dependence for the percentage of over-threshold I_{asym} — the difference between mono- and polyharmonic pulsations varies from ~20 % at $T_1<40$ min to almost twofold at $T_1>80$ min. Thus, in addition to a higher ratio R^2_{IB}, polyharmonic pulsations are characterized by a long lifetime of unipolar GIC of several amperes.
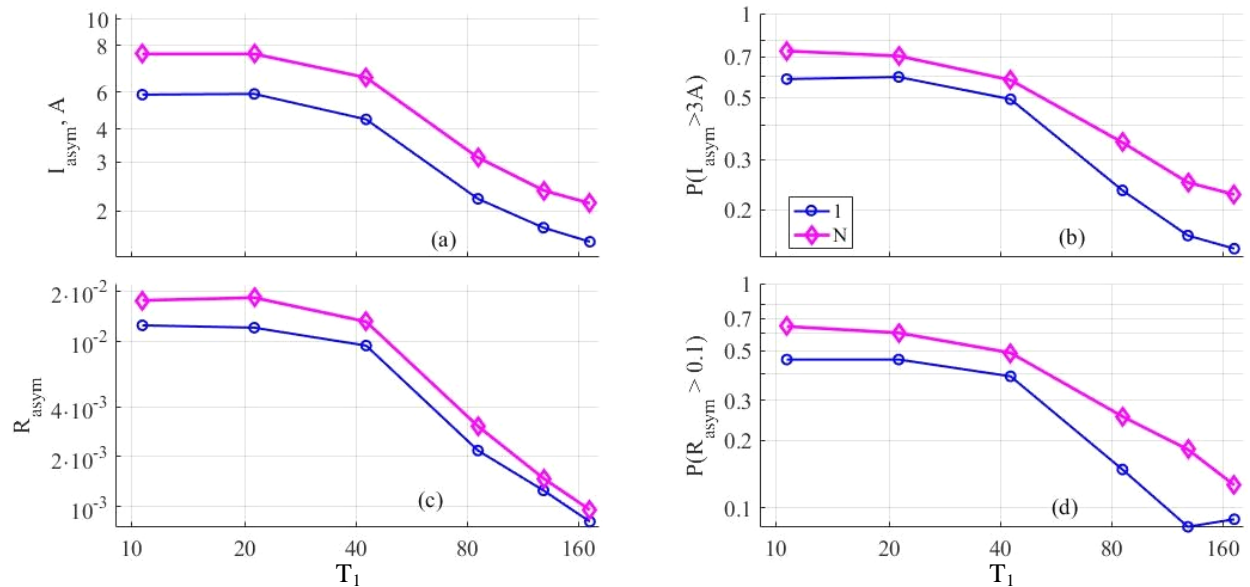

Figure 5. Parameters of the average interval of unipolar GIC I_{asym} as function of the interval length T_1: average $|I_{asym}|$ (*a*); part of the intervals with $|I_{asym}|>3$ A (*b*); the ratio of the R_{asym} value $|I_{asym}|$ to the amplitude of GIC variations (*c*); the probability of $R_{asym}>0.1$ (*d*)

2.4. Conditions for the occurrence of polyharmonic pulsations

Sakharov et al. [2024] have examined conditions outside and inside the magnetosphere favorable for generating pulsations with high GIC efficiency. At the same time, only pulsations in the frequency range to 5 mHz were studied. Inclusion of higher frequencies in the analysis confirmed a great potential hazard of polyharmonic pulsations. This is due to both their greater GIC efficiency and the longer existence times of unipolar GICs. Figure out which conditions are most favorable for the occurrence of polyharmonic pulsations in the range to 20 mHz.

The occurrence frequency of regular Pc3-5 pulsations has dawn and dusk maxima, with the dawn one being more pronounced [Greenstadt et al., 1979; Lee, Olson, 1980]. Figure 6 illustrates diurnal variation in the probability of two pulsation groups in the form of the dependence of the probability density function (PDF) on the magnetic local time (MLT). The principal maximum of the diurnal variation in PDF of monoharmonic pulsations occurs in the dawn sector (6–9 MLT); and two weak maxima, in the dusk (15–18 MLT) and pre-midnight (21–24 MLT) sectors. The first two maxima coincide with those known for Pc3-5 pulsations, and the night one is probably associated with the Pi2 series [Guglielmi and Troitskaya, 1973]. The diurnal variation in the probability of polyharmonic pulsations is smoothed out — there is a wide maximum from 6 to 21 MLT.

Consider whether the generation conditions for these two groups of pulsations differ or not. We use the *Dst* and *AE* indices to measure geomagnetic storms and auroral substorms, and of extra-magnetospheric factors we analyze the absolute value and level of fluctuations in the solar wind dynamic pressure P_{SW}, interplanetary magnetic field component B_z, and the solar wind velocity V. We look at each parameter during the interval $[-\tau, 0]$, where 0 corresponds to the beginning of the detection interval for pulsations of each group. We employ *Dst* minimum for each interval $[-\tau, 0]$ Dst_{min}; and for the remaining parameters, its averages. The results for the two pulsation groups are shown in Figure 7 as a dependence of the parameter considered on the interval length τ.
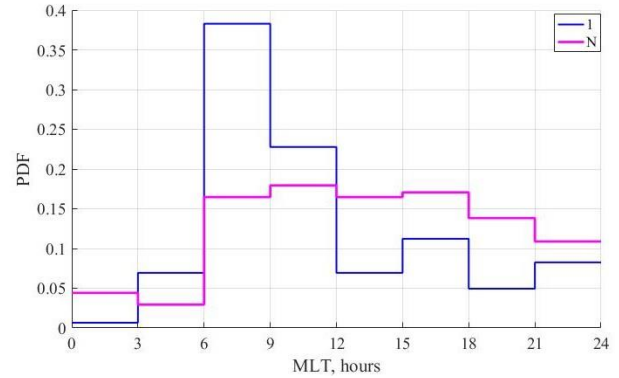

Figure 6. Probability density function (PDF) of the number of intervals with mono and polyharmonic pulsations as function of magnetic local time
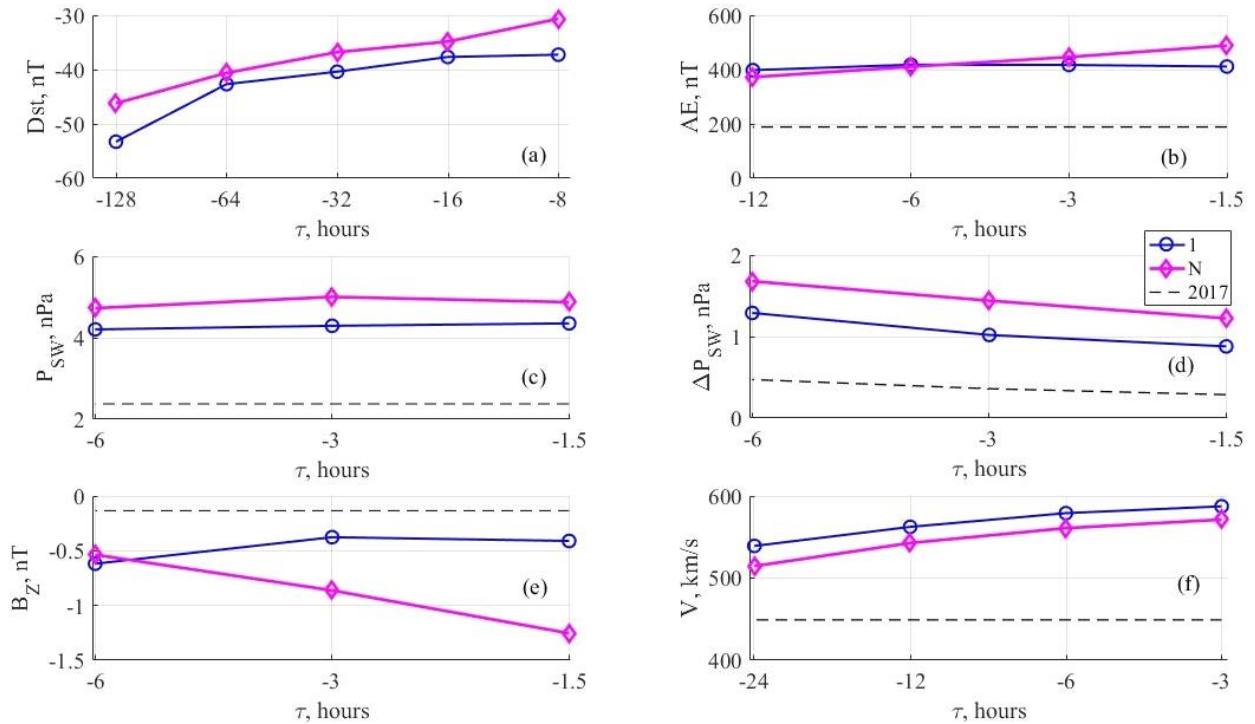

Figure 7. Dependence of geomagnetic activity indices and IMF and SW parameters in the interval $[-\tau, 0]$ on τ, where 0 corresponds to the beginning of the interval when mono and polyharmonic pulsations were detected: minimum *Dst* (*a*); *AE* (*b*); SW dynamic pressure P_{SW} (*c*); amplitude of P_{SW} fluctuations (*d*); IMF B_z (*e*); SW velocity (*f*); dashed lines indicate annual averages

For comparison, Figure 7 also presents annual averages of the parameters under study. Figure 7, *a* exhibits averages of Dst_{min} for two pulsation groups. They correspond to the level of a weak magnetic storm. Polyharmonic pulsations occur on average during weaker storms, and maximum differences between conditions for the two pulsation groups are observed at the smallest and largest τ values. The results for the *AE* index are presented in Figure 7, *b*. Pulsations of both types are observed for higher auroral activity, and differences between the two groups arise only at small τ and are ~100 nT. In both cases, the difference between the conditions for the two pulsation groups is smaller than between annual averages of the parameter and its values when pulsation-related GICs are excited.

Sakharov et al. [2024] have dealt only with the intensity of P_{SW} fluctuations, but we also analyze absolute values of P_{SW} since it defines the position of the magnetopause, which has an effect on the spatial distribution of the Alfvén velocity and hence on the frequency content of pulsations. The P_{SW} values for the intervals when both pulsation groups were observed are higher than the annual average (2.4 nPa), and are 4.2 nPa for monoharmonic pulsations and 4.9 nPa for polyharmonic ones (Figure 7, *c*). A similar pattern is seen for the intensity of P_{SW} fluctuations (Figure 7, *d*): with annual average ΔP_{SW}=0.4 nPa, ΔP_{SW}= 1 nPa for the intervals with monoharmonic pulsations and 1.5 nPa with polyharmonic ones.

The most significant differences between the pulsation groups both in absolute values and in the τ dependence occur for IMF B_z (Figure 7, *e*). With annual average B_z=–0.1 nT for the intervals with monoharmonic pulsations, B_z is –0.4 nT, and for the intervals with polyharmonic ones it varies from –0.5 nT at τ=–6 hrs to –1.3 nT at τ=–1.5 hr.

The results for the solar wind velocity are presented in Figure 7, *f*. With annual average *V*=445 km/s, the SW velocity varies from 540 to 585 km/s for monoharmonic pulsations and from 520 to 570 km/s for polyharmonic ones.

Thus, polyharmonic pulsations occur against the background of greater differences from annual averages than monoharmonic ones, *AE*, IMF B_z, absolute P_{SW} value, and intensity of ΔP_{SW}. For *AE* and B_z, the effect is observed at small τ; whereas for P_{SW} and ΔP_{SW}, at all τ. For the *Dst* index and the solar wind velocity *V*, the opposite situation arises when there are greater differences from the average level for the intervals of detection of monoharmonic pulsations.

3. DISCUSSION

Analysis of GICs associated with geomagnetic pulsations in the 1–20 mHz frequency range has revealed that pulsations at frequencies above 5 mHz are also effective sources of GICs. Polyharmonic pulsations are potentially the most hazardous, in which the frequency of one of the spectral maxima lies above 5 mHz. Physically, this is due to the direct dependence of R_{IB}^2 on

frequency and a fairly high percentage of large-scale pulsations at *f*>5 mHz. Thus, effective monitoring requires GIC measurements with a sampling rate no more than 10 s.

The lifetime of T_1 of the unipolar current I_{asym} of a given intensity is important for the problem of the GIC effect on power transformers, but has not been treated experimentally before. This parameter is higher for polyharmonic pulsations, and the greatest differences are observed for 5–6 A currents such that T_1 is 40–50 min and approximately twice the corresponding index for monoharmonic pulsations.

The probability of GICs associated with pulsations of both groups increases during the magnetic storm recovery phase, but polyharmonic pulsations occur during weaker storms. Pulsations of both groups develop during increased auroral activity, determined both from current *AE* values and by averaging the index over the range [–τ, 0], where τ varies from 1.5 to 12 hrs. Differences between the pulsation groups appear at τ<3 hrs.

Among the solar wind and the interplanetary medium parameters, the solar wind dynamic pressure P_{SW}, the intensity of its fluctuations ΔP_{SW}, and IMF B_z affect the probability of the two pulsation groups. For both pulsation groups, P_{SW} and ΔP_{SW} are higher, and B_z is lower than the annual average ones. An additional enhancement of this effect is observed for polyharmonic pulsations. Given the positive correlation between the amplitudes of fluctuations in P_{SW} and IMF components, the minimum interval of B_z is also lower for polyharmonic pulsations.

Both pulsation groups are observed at higher SW velocities. As it has been found in [Sakharov et al., 2024], the long-term existence of moderately increased velocities is comparable in effect to the short-term existence of a higher velocity. At the same time, high values of *V* (almost 600 km/s) correspond to monoharmonic pulsations. This allows us to explain the saturation effect of the SW velocity on GIC efficiency of pulsations observed in [Sakharov et al., 2024]. The velocities of ~550 km/s are the most favorable for generating polyharmonic pulsations.

Geomagnetic pulsations are generated both by forced oscillations, associated with disturbances of the magnetopause by quasi-periodic variations in P_{SW} and penetration of IMF variations into the magnetosphere, and by a system of oscillations and waves developing inside the magnetosphere. Let us view the discovered regularities of occurrence of the two pulsation groups from this standpoint. Monoharmonic pulsations develop at high solar wind velocities, generally in the dawn sector and during the recovery phase of magnetic storms and auroral substorms. These conditions correspond to the effective occurrence of intramagnetospheric oscillations. Polyharmonic pulsations develop during auroral activations, with a high level of fluctuations in the solar wind dynamic pressure and negative B_z. For them, the diurnal variation features a wide maximum in the daytime. Thus, polyharmonic pulsations occur at high intensity of external fluctuations and under favorable con-

ditions for their penetration into the magnetosphere. This suggests that the contribution of external fluctuations to the pulsations of this group is higher than in the case of monoharmonic pulsations.

In addition to the problem of monitoring potentially hazardous GICs, it is important to predict them for applications. For disturbances with an explicit external trigger in the interplanetary medium, the prediction can be made and implemented both in the form of functional dependences [Temerin, Li, 2006] and by machine learning methods [Tasistro-Hart et al., 2021]. Thus, the methods of predicting a magnetic storm can also be used to predict storm-related GICs, which have been studied most extensively [Kataoka, Pulkkinen, 2008; Schillings et al., 2022]. Prediction of geomagnetic pulsations is less effective [Pilipenko et al., 2023]. This is due to the fact that the amplitude, spectral content, and spatial distribution of the wave field depend significantly on parameters inside the magnetosphere. Analysis of pulsation-associated GICs has shown that these limitations relate more to monoharmonic pulsations. At the same time, polyharmonic pulsations, which are a more effective source of potentially hazardous GICs, also reveal a greater dependence on the level of extra-magnetospheric fluctuations than monoharmonic ones. As a result, it becomes possible in principle to predict parameters of the pulsations of this group and their associated GICs.

CONCLUSIONS

1. GICs are effectively excited by both Pc5/Pi3 geomagnetic pulsations and Pc4/Pi2 higher-frequency pulsations.

2. The most effective source of GICs is polyharmonic pulsations having a spectral maximum at a frequency above 5 mHz.

3. Polyharmonic pulsations lead to the long existence of unipolar GICs, which increases the potential danger of a disturbance of this type to electrical equipment.

4. Favorable conditions for excitation of polyharmonic pulsations generating GICs of over-threshold amplitude are observed during increased auroral activity and/or during the recovery phase of magnetic storms, including weak ones. Such conditions in the interplanetary medium feature southward IMF B_z, the solar wind velocity of 500 to 600 km/s, and increased absolute value and intensity of fluctuations in the solar wind dynamic pressure.

REFERENCES

Apatenkov S.V., Sergeev V.A., Pirjola R., Viljanen A. Evaluation of the geometry of ionospheric current systems related to rapid geomagnetic variations. *Ann. Geophys*. 2004, vol. 22, pp. 63–72. DOI: 10.5194/angeo-22-63-2004.

Barannik M.B., Danilin A.N., Kat'kalov Y.V., Kolobov V.V., Sakharov Y.A., Selivanov V.N. A system for recording geomagnetically induced currents in neutrals of power autotransformers. *Instrum. Exp. Tech*. 2012, vol. 55, pp. 110–115. DOI: 10.1134/S0020441211060121.

Baransky L.N, Fedorov E.N, Kurneva N.A., Pilipenko V.A., Green A.W., Worthington E.W. Gradient and polarization methods of the ground-based hydromagnetic monitoring of magnetospheric plasma. *J. Geomagn. Geolect*. 1995, vol. 47, pp. 1293–1309.

Bedrosian P.A., Love J.J. Mapping geoelectric fields during magnetic storms: Synthetic analysis of empirical United States impedances. *Geophys. Res. Lett*. 2015, vol. 42, pp. 10160–10170. DOI: 10.1002/2015GL066636.

Boteler D.H. A 21st century view of the March 1989 magnetic storm. *Space Weather*. 2019, vol. 17, pp. 1427–1441. DOI: 10.1029/2019SW002278.

Boteler D.H., Pirjola R.J. Modeling geomagnetically induced currents. *Space Weather*. 2017, vol. 15, pp. 258–276. DOI: 10.1002/2016SW001499.

Cherevatova M., Smirnov M.Yu., Korja T., Pedersen L.B., Ebbing J., Gradmann S., Becken M. Electrical conductivity structure of north-west Fennoscandia from three-dimensional inversion of magnetotelluric data. *Tectonophysics*. 2015, vol. 653, pp. 20–32. DOI: 10.1016/j.tecto.2015.01.008.

Fukunishi H., Lanzerotti L.J. ULF pulsation evidence of the plasmapause: 1. Spectral studies of Pc3 and Pc4 pulsations near L=4. *J. Geophys. Res*. 1974, vol. 79, iss. 1, pp. 142–158. DOI: 10.1029/JA079i001p00142.

Gannon J.L., Birchfield A.B., Shetye K.S., Overbye T.J. A comparison of peak electric fields and GICs in the Pacific Northwest using 1-D and 3-D conductivity. *Space Weather*. 2017, vol. 15, pp. 1535–1547. DOI: 10.1002/2017SW001677.

Greenstadt E.W., Singer H.J., Russell C.T., Olson J.V. IMF orientation, solar wind velocity, and Pc3-4 signals: A joint distribution. *J. Geophys. Res*. 1979, vol. 84, iss. A2, pp. 527–532. DOI: 10.1029/JA084iA02p00527.

Guglielmi A.V., Troitskaya V.A. *Geomagnitnye pul'satsii i diagnostika magnitosfery* [Geomagnetic Pulsations and Diagnostics of the Magnetosphere]. Moscow, Nauka Publ., 1973, 208 p. (In Russian).

Gusev Y.P., Lkhamdondog A., Monakov Y.V., Yagova N.V., Pilipenko V.A. Evaluating the effect of geoinduced currents on the startup modes of power transformers. *Power Technol. Eng*. 2020a, vol. 54, pp. 285–290. DOI: 10.1007/s10749-020-01202-1.

Gusev Y.P., Lkhamdondog A., Monakov Y.V., Yagova N.V. Sign-constant current influence on flux linkage balance of power transformer's primary and secondary winding. *Releinaya zashchita i avtomatozatsiya* [Relay protection and automation]. 2020b, iss. 2 (39), pp. 20–25. (In Russian).

Hartinger M.D., Shi X., Lucas G.M., Murphy B.S., Kelbert A., Baker J.B.H., et al. Simultaneous observations of geoelectric and geomagnetic fields produced by magnetospheric ULF waves. *Geophys. Res. Lett*. 2020, vol. 47, iss. 18, E2020GL089441. DOI: 10.1029/2020GL089441.

Hartinger M.D., Shi X., Rodger C.J., Fujii I., Rigler E.J., Kappler K., et al. Determining ULF wave contributions to geomagnetically induced currents: The important role of sampling rate. *Space Weather*. 2023, vol. 21, iss. 5, E2022SW003340. DOI: 10.1029/2022SW003340.

Heyns M.J., Lotz S.I., Gaunt C.T. Geomagnetic pulsations driving geomagnetically induced currents. *Space Weather*. 2021, vol. 19, iss. 2, E2020SW002557. DOI: 10.1029/2020SW002557.

Howard T.A., Menk F.W. Ground observations of high-latitude Pc3-4 ULF waves. *J. Geophys. Res*. 2005, vol. 110, iss. A4, A04205. DOI: 10.1029/2004JA010417.

Jenkins G., Watts D. *Spectral analysis and its applications*. San Francisco, London, Amsterdam, Holden-Day, 1969, 525 p.

Juusola L., Vanhamäki H., Viljanen A., Smirnov M. Induced currents due to 3D ground conductivity play a major

role in the interpretation of geomagnetic variations. *Ann. Geophys*. 2020, vol. 38, pp. 983–998. DOI: 10.5194/angeo-38-983-2020.

Kataoka R., Pulkkinen A. Geomagnetically induced currents during intense storms driven by coronal mass ejections and corotating interacting regions. *J. Geophys. Res*. 2008, vol. 113, iss. A3, A03S12. DOI: 10.1029/2007JA012487.

Lee L.C., Olson J.V. Kelvin-Helmholtz instability and the variation of geomagnetic pulsation activity. *Geophys. Res. Lett.* 1980, vol. 7, pp. 777–780. DOI: 10.1029/GL007i010p00777.

Lifshicz A.E, Fedorov E.N. Hydromagnetic oscillations of the magnetosphere-ionosphere resonator. *Doklady AN SSSR* [Reports of the USSR Academy of Sciences]. 1986, vol. 287, pp. 90–95. (In Russian.)

Lotz S.I., Danskin D.W. Extreme value analysis of induced geoelectric field in South Africa. *Space Weather*. 2017, vol. 15, iss. 10, pp. 1347–1356. DOI: 10.1002/2017SW001662.

Love J.J., Coisson P., Pulkkinen A. Global statistical maps of extreme-event magnetic observatory 1 min first differences in horizontal intensity. *Geophys. Res. Lett*. 2016, vol. 43, iss. 9, pp. 4126–4135. DOI: 10.1002/2016GL068664.

Love J.J., Lucas G.M., Rigler E.J., Murphy B.S., Kelbert A., Bedrosian P.A. Mapping a magnetic superstorm: March 1989 geoelectric hazards and impacts on United States power systems. *Space Weather*. 2022, vol. 20, e2021SW003030. DOI: 10.1029/2021SW003030.

Marshall R.A., Dalzell M., Waters C.L., Goldthorpe P., Smith E.A. Geomagnetically induced currents in the New Zealand power network. *Space Weather*. 2012, vol. 10, S08003. DOI: 10.1029/2012SW000806.

Motoba T., Takahashi K., Rodriguez J.V., Russell C.T. Giant pulsations on the afternoonside: Geostationary satellite and ground observations. *J. Geophys. Res.: Space Phys*. 2015, vol. 120, pp. 8350–8367. DOI: 10.1002/2015JA021592.

Nakamura S., Ebihara Y., Fujita S., Goto T., Yamada N., Watari S., Omura Y. Time domain simulation of geomagnetically induced current (GIC) flowing in 500-kV power grid in Japan including a three-dimensional ground inhomogeneity. *Space Weather*. 2018, vol. 16, pp. 1946–1959. DOI: 10.1029/2018SW002004.

Nosé M., Liou K., Sutcliffe P.R. Longitudinal dependence of characteristics of low-latitude Pi2 pulsations observed at Kakioka and Hermanus. *Earth Planet Space*. 2006, vol. 58, pp. 775–783. DOI: 10.1186/BF03351981.

Pilipenko V., Kozyreva O., Hartinger M., Rastaetter L., Sakharov Ya. Is the global MHD modeling of the magnetosphere adequate for GIC prediction: the May 27–28, 2017 storm. *Cosmic Res*. 2023, vol. 61, pp. 120–132. DOI: 10.1134/S0010952522600044.

Pulkkinen A., Lindahl S., Viljanen A., Pirjola R. Geomagnetic storm of 29–31 October 2003: Geomagnetically induced currents and their relation to problems in the Swedish high-voltage power transmission system. *Space Weather*. 2005, vol. 3, S08C03. DOI: 10.1029/2004SW000123.

Pulkkinen A., Klimas A., Vassiliadis D., Uritsky V., Tanskanen E. Spatiotemporal scaling properties of the ground geomagnetic field variations. *J. Geophys. Res*. 2006, vol. 111, A03305. DOI: 10.1029/ 2005JA011294.

Pulkkinen A., Pirjola R., Viljanen A. Statistics of extreme geomagnetically induced current events. *Space Weather*. 2008, vol. 6, S07001. DOI: 10.1029/2008SW000388.

Sakharov Y.A., Yagova N.V., Pilipenko V.A. Pc5/Pi3 geomagnetic pulsations and geomagnetically induced currents. *Bull. Russian Acad. Sci. Phys*. 2021, vol. 85, pp. 329–333. DOI: 10.3103/S1062873821030217.

Sakharov Ya.A., Yagova N.V., Pilipenko V.A., Selivanov V.N. Spectral content of Pc5–6/Pi3 geomagnetic pulsations and their efficiency in generation of geomagnetically induced currents. *Russ. J. Earth. Sci*. 2022, vol. 22, ES1002. DOI: 10.2205/2021ES000785.

Sakharov Ya.A., Yagova N.V., Bilin V.A., Selivanov V.N., Aksenovich T.V., Pilipenko V.A. Parameters influencing the efficiency of generation of geomagnetically induced currents by nonstorm Pc5–6/Pi3 geomagnetic pulsations. *Bull. Russian Acad. Sci. Phys*. 2024, vol. 88, pp. 289–295. DOI: 10.1134/S1062873823705421.

Schillings A., Palin L., Opgenoorth H.J., Hamrin M., Rosenqvist L., Gjerloev J.W., Juusova L., Barnes R. Distribution and occurrence frequency of dB/dt spikes during magnetic storms 1980–2020. *Space Weather*. 2022, vol. 20, E2021SW002953. DOI: 10.1029/ 2021SW002953.

Tanskanen E.I. A comprehensive high-throughput analysis of substorms observed by IMAGE magnetometer network: Years 1993–2003 examined. *J. Geophys. Res*. 2009, vol. 114, A05204. DOI: 10.1029/2008JA013682.

Tasistro-Hart A., Grayver A., Kuvshinov A. Probabilistic geomagnetic storm forecasting via deep learning. *J. Geophys. Res.: Space Phys*. 2021, vol. 126, E2020JA028228. DOI: 10.1029/ 2020JA028228.

Temerin M., Li X. *Dst* model for 1995–2002. *J. Geophys. Res*. 2006, vol. 111, A04221. DOI: 10.1029/2005JA011257.

Trichtchenko L. Frequency considerations in GIC applications *Space Weather*. 2021, vol. 19, E2020SW002694. DOI: 10.1029/2020SW002694.

Wang G.Q., Volwerk M., Zhang T.L., Schmid D., Yoshikawa A. High-latitude Pi2 pulsations associated with kink-like neutral sheet oscillations. *J. Geophys. Res.: Space Phys*. 2017, vol. 122, pp. 2889–2899. DOI: 10.1002/2016JA023370.

Wik M., Viljanen A., Pirjola R., Pulkkinen A., Wintoft P., Lundstedt H. Calculation of geomagnetically induced currents in the 400 kV power grid in southern Sweden. *Space Weather*. 2008, vol. 6, S07005. DOI: 10.1029/ 2007SW000343.

Yagova N.V., Pilipenko V.A., Sakharov Y.A., Selivanov V.N. Spatial scale of geomagnetic Pc5/Pi3 pulsations as a factor of their efficiency in generation of geomagnetically induced currents. *Earth Planets Space*. 2021, vol. 73, art. no. 88. DOI: 10.1186/s40623-021-01407-2.

Yumoto K., Osaki H., Fukao K., Shiokawa K., Tanaka Y., Solovyev S.I., Krymskij G., Vershinin E.F., Osinin V.F. and 210 MM Magnetic Observation Group. Correlation of high- and low-latitude Pi2 magnetic pulsations observed at 210 magnetic meridian chain stations. *J. Geomagn. Geoelectr*. 1994, vol. 46, pp. 925–935. DOI: 10.5636/jgg.46.925.

Zhang T., Ebihara Y. Superposed epoch analyses of geoelectric field disturbances in Japan in response to different geomagnetic activities. *Space Weather*. 2022, vol. 20, E2021SW002893. DOI: 10.1029/2021SW002893.

How to cite this article
Yagova N.V., Sakharov Ya.A., Pilipenko V.A., Selivanov V.N. Long-period geomagnetic pulsations as an element of the space weather influence on technological systems. *Solar-Terrestrial Physics*. 2024. Vol. 10. Iss. 3. P. 137–146. DOI: 10.12737/stp-103202415.